About the determination of the representative volume element size in compact bone.

(Sur le volume élémentaire représentatif à considérer pour la modélisation de l'os compact.)

QUENTIN GRIMAL[a], KAY RAUM[b], ALF GERISCH[c] AND PASCAL LAUGIER[a]

a. Université Pierre et Marie Curie-Paris6, Laboratoire d'Imagerie Paramétrique, Paris, F-75005 France; CNRS, LIP, Paris, F-75006 France
b. Q-BAM Group, Dept. of Orthopedics Martin-Luther-Universität Halle-Wittenberg, Magdeburger Straße 22, 06097 Halle (Saale), Germany
c. Institut für Mathematik Martin-Luther-Universität Halle-Wittenberg, Postfach D-06099 Halle (Saale), Germany

Résumé :

L'os cortical est essentiellement biphasique (pores+matrice). Pour le calcul de propriétés effectives, il faut choisir un volume élémentaire représentatif (VER). Ce choix est délicat car 1) le tissu est hétérogène à plusieurs échelles (i.e. zones plus ou moins poreuses en moyenne) ; 2) la couche corticale peut être très fine. Nous montrerons que le choix d'un VER de taille millimétrique peut permettre de calculer de manière satisfaisante des propriétés effectives.

Abstract :

Corical bone is essentially a biphasic composite material (mineralized matrix + pores). In order to calculate effective properties a representative volume element (RVE) needs to be defined. The choice of the size of the RVE is difficult because: (i) bone material is heterogeneous (variation of porosity in the cortical shell); (ii) the thickness of the cortical shell is small. It is shown that an RVE size in the millimeter range may actually be used to calculate effective properties with a limited precision.

Mots clefs : os, homogénéisation, volume élémentaire représentatif

1 Introduction

Cortical bone is a well-organized hard tissue which represents approximately 80 % of the skeletal mass in the human adult. It can be described as a two-phase composite material: a dense mineralized matrix and a soft phase, i.e. pores containing fluid and soft tissues. Cortical bone tissue is a multi-scale material with different characteristic microstructural patterns from the nanometer to the millimeter scales. Porosity is distributed over several length scales: the diameter of pores range from a few micrometers to several hundreds of micrometers [13]. Resorption cavities (approximately $50 - 200\ \mu m$) and Haversian canals (approximately $50\ \mu m$) are characteristic of the higher level of organization in bone. These pores are roughly aligned with the longitudinal direction of bone [4, 2] and embedded in the matrix which is a mixture of the smaller pores (at least one order of magnitude smaller than resorption cavities and Haversian canals) and mineralized collagen fibrils.

In the framework of continuum mechanics [6], each material point is a volume of a homogeneous material which is mathematically shrunk to zero from the macroscopic point of view but which represents a volume of finite microscopic dimension with a microstructure. Accordingly, the concept of material point is associated to the concept of *representative volume element* (RVE). For a non-periodic microstructure, the RVE is defined as a volume containing a very large (mathematically infinite) number of microscale elements [14, p. 237]. This definition is valid, in principle, only for the case of a statistically homogeneous and ergodic material. In what follows we will make reference to three scales and their characteristic dimension: the microscale of characteristic dimension d, typically the scale of Haversian channels and resorption cavities (around $100\ \mu m$); the mesoscale with characteristic dimension denoted L; the macroscale with characteristic dimension denoted L_{macro} which is the size of the macroscopic body, typically $0.5 - 10\ mm$ for the cortical shell thickness of a long bone. In continuum mechanics, the statement of separation of scales is [14]

$$d < L \ll L_{macro} \quad or \quad d \ll L \ll L_{macro}. \tag{1}$$

The mesoscale appears to be an intermediate scale; for the mesoscale to be actually separated from the microscale, L should be at least as large as the RVE: $L \geq L_{RVE}$. If the microstructure has a weak disorder and/or a

weak mismatch in properties, the inequality $d < L$ may be sufficient; otherwise $d \ll L$ applies. The issue of central concern is how fast the *apparent* mesoscale homogenized properties approach the *effective* response of the RVE, i.e. macroscopic elastic properties, with increasing values of the ratio L/d.

Recently, the mesoscale of cortical bone has been given particular attention [11, 9, 1] in association to novel experimental techniques such as nanoindentation [21], syncrhotron X-Ray computed tomography, and quantitative scanning acoustic microscopy [17]. These techniques enable the explicit description of the mesoscopic domains in terms of geometry (microstructure) and/or distribution of local elastic properties. The characteristic size of RVE in cortical bone is considered to be in the millimeter range since a millimetric volume includes several resorption cavities and Haversian canals and is usually smaller than the thickness of the cortical shell. However the more restrictive statement of scale separation: $d \ll L \ll L_{macro}$ can hardly be met in cortical bone for which the ratio d/L_{macro} is approximately bounded as $1/100 < d/L_{macro} < 1/5$ for a large thickness ($10\ mm$) and a small thickness ($0.5\ mm$), respectively. In addition gradients of porosity are commonly observed in cortical bone, leading to mesoscopic heterogeneity, i.e a variation of the mesoscopic response from points to points. To the authors's knowledge, it is yet unknown whether the statement of separation of scales applies in practice for cortical bone; in other words the minimum size L of a mesodomain such that $L \geq L_{RVE}$ is not known. Several authors have attempted to estimate millimeter scale elastic properties based on idealized and virtually unbounded geometry of the osteonal pattern. For instance in references [3, 19, 5, 15], authors either considered periodic or, alternatively, random microstructures and assumed the separation of scale to be valid. In the latter works, homogenization of bone elastic properties have been conducted following a *deterministic* approach assuming that there actually exists a mesodomain of bone tissue of size L such that $L \geq L_{RVE}$. In fact authors have assumed that homogenized bone properties can be uniquely defined. According to Hill [10, 14], the homogenized properties of a mesodomain of size L are unique only in the case $L \geq L_{RVE}$; in that case the homogenized properties are "independent of the surface values of traction or displacement, so long as these values are macroscopically uniform", in other words, the elastic response is independent of the boundary conditions applied on the mesodomain. A detailed analysis of the conditions for scale separation in bone material is lacking. As a consequence, the applicability of the effective properties estimations based on homogenization models is unclear.

The work presented in this paper is a contribution to the definition of the RVE size for cortical bone. The specific aim of the paper is to determine the evolution of the apparent mesoscale elastic response with increasing mesodomain size L. At the limit of large L ($d \ll L$), the apparent properties of a mesodomain of size $L \geq L_{RVE}$ should equal the macroscopic effective properties. The apparent elastic response of mesodomains subjected to different boundary conditions (BCs) were computed for different mesodomain sizes. With this approach, the RVE size may be defined as the mesodomain size for which apparent elastic properties become weakly dependent on the BCs type used. Our approach is similar to those followed for various types of microstructures, see e.g., [18, 20, 16]. A model of cortical bone mesoscopic properties coupled to quantitative images of bone tissue [9] is used to generate mesodomains with different sizes. The model is particularly well suited to the determination of the RVE size for cortical bone because is accounts for the realistic heterogeneity of bone at the microscale.

2 Method

One square image of 3 mm edge size (see Figure 1) of cortical bone tissue was extracted from the image of a cross-section of a human femur. The 3 mm^2 area within the femur cross-section was chosen so that the homogeneity of the microstructure was maximized to the first authors's eye. In particular, areas including very large pores or an obvious porosity gradient were avoided. Note that it was not possible to obtain an image much larger than 3 mm edge size with a sufficiently homogeneous microstructure. The image was obtained with 50 MHz scanning acoustic microscopy (SAM) [17] for the purposes of another study. The direction of the bone axis (diaphysis) was taken parallel to axis $\mathbf{x_3}$ and the cross-section was assumed to be in the plane ($\mathbf{x_1}$,$\mathbf{x_2}$). The scanning acoustic microscope had a physical resolution of 23 μm and the image resolution (pixel size) was 16 μm. Each pixel of the SAM image is associated to a value of acoustic impedance representative of the tissue elasticity [17]. With the resolution used, only the largest pores (Haversian channels, resorption cavities) are actually resolved; the smallest pores (Volkmann's canal, osteocyte lacunae, etc.) cannot be distinguished from the matrix so that they contribute to the bulk matrix properties probed. The sample had a mean porosity of 8.5 % which is typical for human cortical bone [4].

A large "parent" image of $9 \times 9\ mm^2$ was constructed based on the $3 \times 3\ mm^2$ impedance image. The latter was duplicated to pad a surface made of nine $3 \times 3\ mm^2$ images. The padding was achieved by assembling along each of the four sides of the $3 \times 3\ mm^2$ image the symmetric image with respect to the side; images in the corner of the padding were obtained by taking the symmetric image with respect to each corner of the $3 \times 3\ mm^2$ image. With this procedure, the central image of the padding is the initial $3 \times 3\ mm^2$ image. The microstructure of the $9 \times 9\ mm^2$ image was assumed to be representative of bone microstructure. Surface padding using symmetry rather than translation ensured that there was no discontinuity in the $9 \times 9\ mm^2$ microstructure. Four sets of $N^{(i)}$ $(i = 1..4)$ square "children" images with different edge sizes $L^{(i)}$ were extracted randomly from the parent image, see table 1. To obtain one children image k, (1) a coordinate point $(x_k^{(i)}, y_k^{(i)})$ was selected randomly within the central image of the padding; (2) a square image with edge size

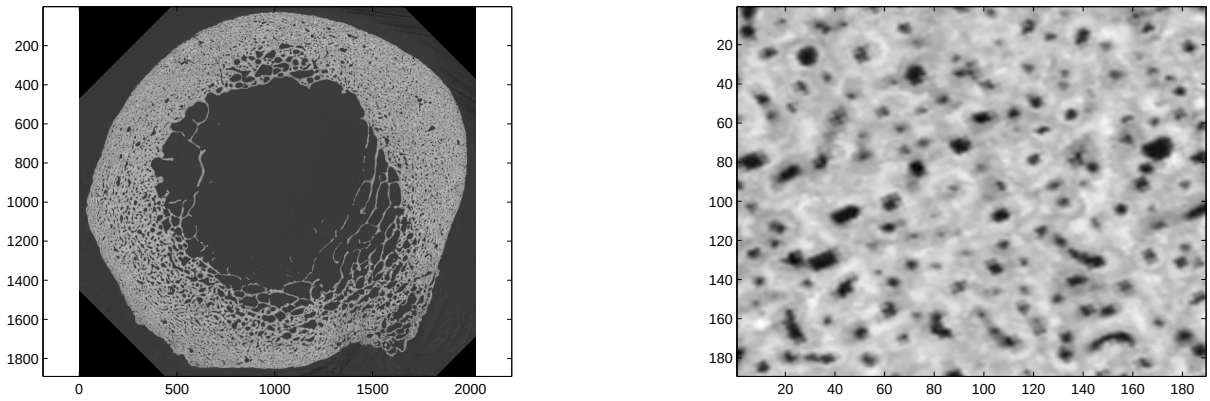

FIG. 1 – *Left: acoustic impedance image (SAM, 23 μm resolution) of a human femur cross-section. Right: image of area approximately $3 \times 3mm^2$ from which smaller children images were extracted. The numbers are pixel numbers; size of pixel is $16 \times 16\mu m^2$.*

L^i and with center $(x_k^{(i)}, y_k^{(i)})$ and randomly chosen orientation angle $\theta_k^{(i)}$ was extracted. Each children image was then extruded in direction x_3 so as to form a parallelepipedic realization of volume $\left(L^{(i)}\right)^2 \times L_3$, where L_3 is the volume dimension in direction x_3. Computation were performed for $L_3 = 0.5\ mm$. Following Kanit et al. [12] each mesodomain realization may be considered as a microstructure realization from a distinct bone sample with the same overall properties as the parent image.

TAB. 1 – *Definition of mesodomain sets*

Characteristic size of mesodomain ($L^{(i)}$, mm)	0.5	1	1.5	2
Number of realizations $N^{(i)}$	60	50	20	20

The impedance data contained in each mesodomain was converted to elasticity values following a procedure described in [9]. Briefly, (1) pixels in pores were segmented from the pixels in the bone matrix and associated with the elastic properties of bulk water (undrained); (2) pixels in matrix were associated with a transverse isotropic stiffness tensor (with (x_1, x_2) being the isotropy plane) representative of bone tissue and dependent on the pixel impedance value.

The apparent properties of each mesodomain were computed using a finite-element based upscaling procedure. The mesodomain was subjected successively to six sets of uniform tractions (hTrac) or uniform displacements (hDisp) boundary conditions (see e.g. [20] for a description of the classical procedure). Stress and strain fields in each mesodomain were calculted with a commercial finite element code (Comsol Multiphysics) in the framework of linearized elasticity. In order to avoid unphysical edge effects due to the possible presence of pores at the mesodomain boundary, the mesodomains were surrounded with a thin layer of thickness $0.05\ mm$ with elastic properties close to the searched apparent properties of the mesodomain. The layer properties were estimated based on empirical relationships from mean porosity and mean elasticity values in the mesodomain [8]. The columns of the apparent stiffness (hDisp) or compliance (hTrac) tensors where finally obtained by dividing components of strain and stress fields [20, 9]. The computed apparent stiffness tensors of a mesodomain corresponds to a material symmetric with respect to the plane (x_1, x_2); however it is close to hexagonal symmetry with x_3 as the axis of symmetry, due to the distribution of pores and transverse isotropy of the matrix. Accordingly the closest transversely isotropic (hexagonal) stiffness tensor of each 'raw' apparent stiffness tensors was calculated following a procedure described in [7, 9]. Finally for each mesodomain, two transverse isotropic apparent stiffness tensors are obtained, associated to hTrac ($\mathbb{C}_{tr}$) and hDisp ($\mathbb{C}_d$) boundary conditions.

Apparent tensors $\mathbb{C}_{tr}$ and $\mathbb{C}_d$ provide lower and upper bounds, respectively, for any other apparent tensor $\mathbb{C}$ of the mesodomain that may be calculated with any type of boundary condition (see e.g. [20, 14]). This means that the eigenvalues of $(\mathbb{C}_d - \mathbb{C})$ and $(\mathbb{C} - \mathbb{C}_{tr})$ are all positive. We introduce the tensor norm $n(\mathbb{A}) = \sqrt{\sum_{i=1..6} \lambda(\mathbb{A})_i^2}$, where $\lambda(\mathbb{A})_i$ $(i = 1..6)$ denote the six eigenvalues of the tensor $\mathbb{A}$. The quantity $\delta = n(\mathbb{C}_d) - n(\mathbb{C}_{tr})$ is always positive and is a suitable scalar measure of the interval between the bounds. The quantity $\delta^k = n(\mathbb{C}_d^k) - n(\mathbb{C}_{tr}^k)$ was calculated for each mesodomain realization k. From each tensor $\mathbb{C}_d^k$ and $\mathbb{C}_{tr}^k$, we calculated Young moduli $E_{l;d,tr}^k$ and $E_{t;d,tr}^k$ and shear coefficients $G_{lt;d,tr}^k$ and $G_{tt;d,tr}^k$, where l and t correspond to directions $\mathbf{x}_3$ and $\mathbf{x}_1$ (or equivalently $\mathbf{x}_2$), respectively. The differences between engineering coefficients

estimated with hDisp and hTrac boundary conditions are defined as

$$g_1 = E_{l;d} - E_{l;tr} \; ; \quad g_2 = E_{t;d} - E_{t;tr} \; ; \quad g_3 = G_{lt;d} - E_{l;tr} \; ; \quad g_4 = G_{tt;d} - E_{l;tr}. \tag{2}$$

Similarly to δ^k, it is expected that the quantities g_i^k $(i = 1..4)$ calculated for each mesodomain be positive and be suitable measures of the dispersion of apparent properties that may be obtained from different types of boundary conditions.

3 Results

Figure 3 displays E_t for all tested mesodomains realizations. The corresponding plots for other engineering coefficients (not shown) were qualitatively similar. The plots illustrate both the dispersion on the apparent modulus value and the dispersion of the gap $g_1(k)$.

The data on the relative gap between apparent properties calculated with hTrac and hDisp boundary conditions is synthesized in figure 3. The figure shows: (i) the mean relative gaps $g_i(k)$ calculated for the 25 % largest gap values; (ii) the mean relative value of δ calculated for the 25 % largest gap values (right).

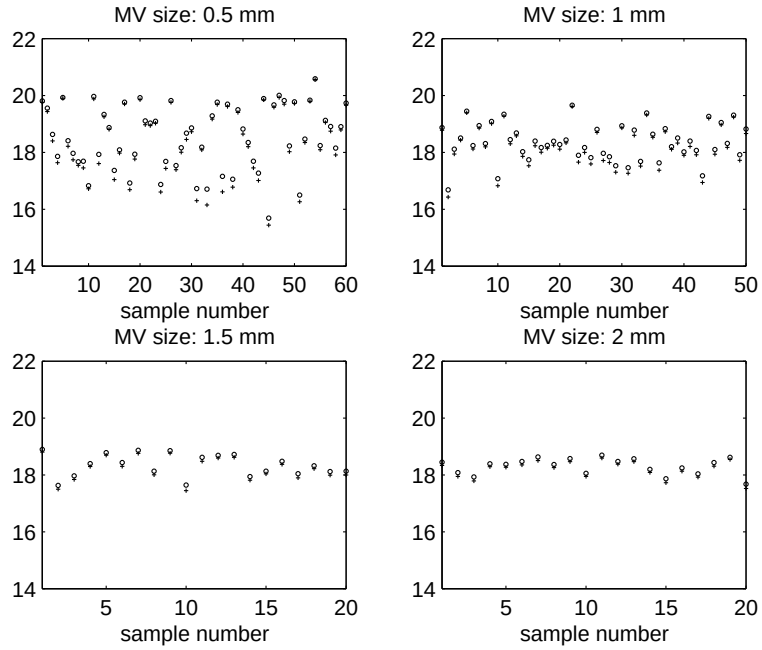

FIG. 2 – *Computed transverse elastic modulus (E_t, GPa) for all microstructure realizations for different mesodomain (material volume, MV) sizes. Boundary conditions hDisp (circle) and hTrac (+).*

4 Discussion and conclusion

The data presented above was considered to discuss the size of the RVE in human cortical bone. The RVE size is defined as the minimum mesodomain size L for which apparent properties become weakly sensitive to the type of boundary condition. The sensitivity of the computed apparent properties to boundary conditions is quantified with δ and g_i $(i = 1..4)$ which are measures of the distance between the bounds of the elastic behavior, for the stiffness tensor itself and the engineering moduli, respectively. Consequently δ and g_i are suitable measures of the closeness of a mesodomain size to the RVE size.

There is a wide distribution of gap values $g_i(k)$, as shown for E_t in figure 3. The smaller the mesodomain, the wider the distribution. Interestingly, the smaller gaps are reached for the smaller volumes; in fact the small gaps correspond to samples with a rather homogeneous distribution of properties (e.g. samples 1, 5, 54, see figure 4), i.e. low porosity. The largest gaps (e.g. samples 12, 24, 33, see figure 5) correspond to samples including a large pore or high heterogeneity. This indicates that in areas where the porosity is low, a very limited volume of tissue can be considered as a locally representative volume (RVE) for which effective properties can actually be estimated locally. For areas with larger porosity, effective properties can not be defined with mesodomain size 0.5 mm.

Because the gap values are scattered, it is not meaningfull to compare the mean gap value for the different mesodomain sizes; as a matter of fact the mean gaps estimated from the whole distributions are not strongly affected by the mesodomain size. It appears to be more relevant to look for a mesodomain size for which a sufficient number of realizations (high probability) will have a small gap. To obtain the data of figure 3 we calculated the average gap for the 25 % samples with higher gap values. This is a simple procedure to quantify the error. Nevetheless other quantitification may be used. Figure 3 reveals the same trend for all four

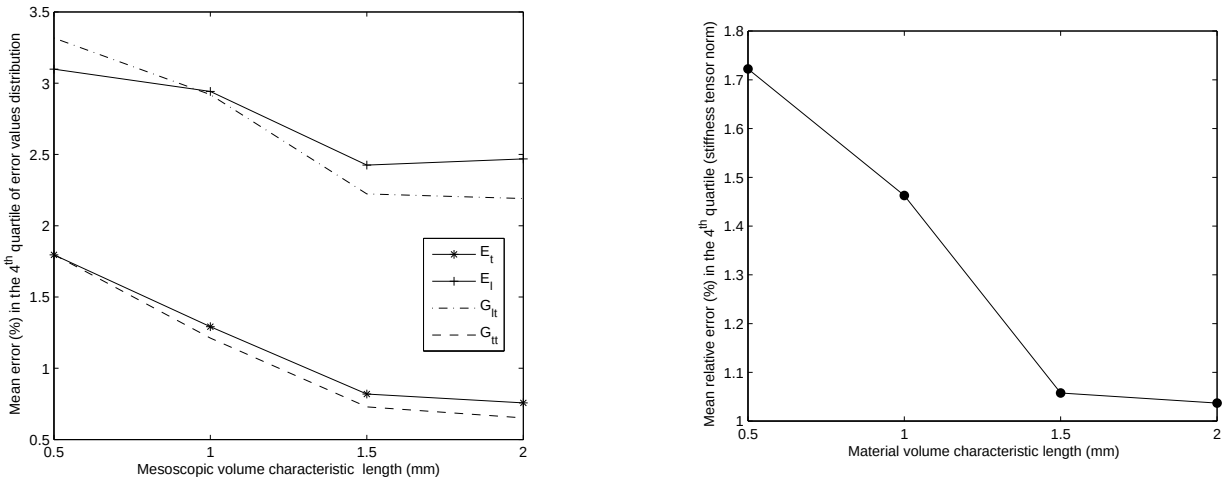

FIG. 3 – *Left: Mean relative difference (%) between apparent engineering moduli obtained with hDisp and hTrac boundary conditions for increasing size of mesodomains; Right: mean relative difference of the norms of apparent tensors obtained with hDisp and hTrac boundary conditions for increasing size of mesodomains. The means were calculated for the values in the* 4^{th} *quartile of values distribution, i.e. on the 25 % largest gaps.*

engineering coefficients and differences in tensor norms. The gap decreases rapidly between 0.5 and 1.5 mm and seems to reach a plateau. There is no reason to believe that calculation with mesodomain sizes in the same range of values (0.5-2 mm) would contradict this conclusion.

The notion of representative volume element is associated to a desired precision on the estimation of effective properties. In view of the different sources of error (computational, experimental data, etc.) the level of precision required on the RVE definition can be assessed. Compared to most other areas of engineering sciences, the level of precision of models in the biomechanics field is less. Typically under 10 % error between model prediction and reference experimental data is often considered as a good result. Even for the smallest mesodomain considered in this work (0.5 mm) the uncertainty on the homogenized elastic response due to boundary condition effects may be considered small enough (below 5 %). However, the scattering of apparent properties due to the fluctuation of the mesodomain content may be considered important. This scattering becomes smaller for mesodomain size 1.5 mm and 2 mm.

The results presented in the paper suggest that for a size as small as 0.5 mm it may be meaningful to calculate effective properties providing these are calculated based on the *local* content of the mesodomain volume, which undergoes important fluctuations from points to points. The uncertainty due to boundary conditions is small, especially for mesodomain sizes 1.5 mm and 2 mm for which homogenized properties may be considered as unique.

Only one bone sample was used for the purposes of the study. The sample was assumed to be representative of human cortical bone tissue. Nevertheless the results of the present study should be supplemented with computation based on other parent microstructures. Finally, the mesodomains used to estimate apparent properties were constructed by extruding a 2D image. This procedure neglects all 3D effects in the porous network. Nevertheless, the approach followed is consistent with that followed for most cortical bone models. Three-dimensional images of cortical bone obtained with synchrotron computed tomography could be used to conduct similar studies with 3D bone models.

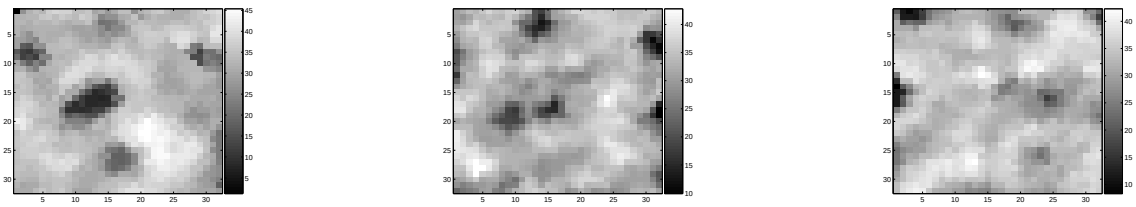

FIG. 4 – *Samples with weak heterogeneity. From left to right (% porosity): sample 1 (4.4 %), 5 (2.2 %) and 54 (1.6 %). of smales with low heterogeneity*

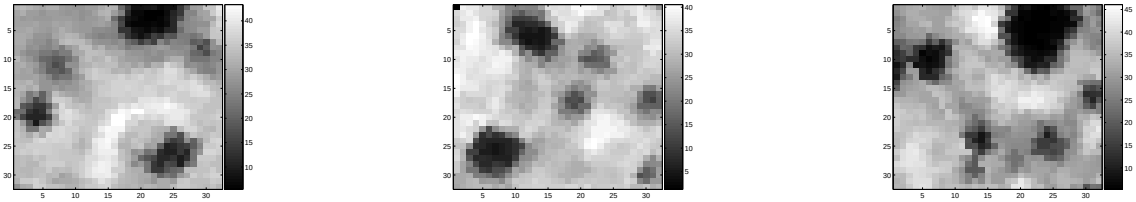

FIG. 5 – *Samples with high heterogeneity. From left to right (% porosity): sample 12 (9.6 %), 24 (12.7 %) and 33 (16.9 %).*

Références

[1] C. Baron, M. Talmant, and P. Laugier. Effect of porosity on effective diagonal stiffness coefficients (cii) and elastic anisotropy of cortical bone at 1 mhz: a finite-difference time domain study. *J Acoust Soc Am*, 122(3):1810, 2007.

[2] David M.L. Cooper, C. David L. Thomas, John G. Clement, Andrei L. Turinsky, Christoph W. Sensen, and Benedikt Hallgrimsson. Age-dependent change in the 3d structure of cortical porosity at the human femoral midshaft. *Bone*, 40(4):957–965, 2007. TY - JOUR.

[3] J. M. Crolet, B. Aoubiza, and A. Meunier. Compact bone: numerical simulation of mechanical characteristics. *Journal of Biomechanics*, 26(6):677–87., 1993.

[4] J.D. Currey. *Bones: Structure and Mechanics*. Princeton Academic Press, 2002.

[5] X. N. Dong and X. E. Guo. Prediction of cortical bone elastic constants by a two-level micromechanical model using a generalized self-consistent method. *Journal of Biomechanical Engineering-Transactions of the Asme*, 128(3):309–316, 2006.

[6] A.C. Eringen. *Mechanics of continua*. John Wiley and Sons, inc, New York, 1967.

[7] M. François, G. Geymonat, and Y. Berthaud. Determination of the symmetries of an experimentally determined stiffness tensor: Application to acoustic measurements. *International Journal of Solids and Structures*, 35(31-32):4091–4106, 1998.

[8] Q Grimal, K Raum, A. Gerisch, and P Laugier. Computation of the overall anisotropic elasticity of cortical bone from micro-scale quantitative acoustic images. In *Congrès Français de Mécanique*, Grenoble, 2007.

[9] Q. Grimal, K. Raum, A. Gerisch, and P. Laugier. Derivation of the mesoscopic elasticity tensor of cortical bone from quantitative impedance images at the micron scale. *Comput Methods Biomech Biomed Engin*, 11(2):147–57, 2008.

[10] R. Hill. Elastic properties of reinforced solids: some theoretical principles. *J. Mech. Phys. Solids*, 11:357, 1963.

[11] T. Hoc, L. Henry, M. Verdier, D. Aubry, L. Sedel, and A. Meunier. Effect of microstructure on the mechanical properties of haversian cortical bone. *Bone*, 38(4):466–474, 2006.

[12] T. Kanit, S. Forest, I. Galliet, V. Mounoury, and D. Jeulin. Determination of the size of the representative volume element for random composites: statistical and numerical approach. *International Journal of Solids and Structures*, 40(13-14):3647–3679, 2003. Times Cited: 64.

[13] R. B. Martin, D. B. Burr, and N. A. Sharkey. *Skeletal Tissue Mechanics*, volume 1. Springer, New York, first edition, 1998.

[14] M. Ostoja-Starzewski. *Microstructural randomness and scaling in mechanics of materials*. Chapman and Hall, CRC, 2008.

[15] W. J. Parnell and Q. Grimal. The influence of mesoscale porosity on cortical bone anisotropy. investigations via asymptotic homogenization. *J R Soc Interface*, 2008.

[16] V. Pensee and Q.-C. He. Generalized self-consistent estimation of the apparent isotropic elastic moduli and minimum representative volume element size of heterogeneous media. *International Journal of Solids and Structures*, 44(7-8):2225–2243, 2007.

[17] K. Raum. Microelastic imaging of bone. *IEEE Trans Ultrason Ferroelectr Freq Control*, 55(7):1417–31, 2008.

[18] K. Sab. On the homogenization and the simulation of random materials. *Europ. J. Mech., A Solids*, 11:585–607, 1992.

[19] I. Sevostianov and M. Kachanov. Impact of the porous microstructure on the overall elastic properties of the osteonal cortical bone. *Journal of Biomechanics*, 33(7):881–888, 2000.

[20] T.I. Zohdi and P. Wriggers. *Introduction to computational micromechanics*. Lecture notes in applied computational mechanics. Springer-Verlag, Berlin, 2005.

[21] P. K. Zysset, X. E. Guo, C. E. Hoffler, K. E. Moore, and S. A. Goldstein. Elastic modulus and hardness of cortical and trabecular bone lamellae measured by nanoindentation in the human femur. *Journal of Biomechanics*, 32(10):1005–12, 1999.